HHS Public Access

Author manuscript

Hear Res. Author manuscript; available in PMC 2018 April 01.

Published in final edited form as:

Hear Res. 2017 April ; 347: 28–40. doi:10.1016/j.heares.2016.10.021.

Plastic changes along auditory pathway during salicylate-induced ototoxicity: Hyperactivity and CF shifts

Chen Jiang[a,b], **Bin Luo**[a,b], **Senthilvelan Manohar**[b], **Guang-Di Chen**[b,*], and **Richard Salvi**[b]

[a]Department of Neurosurgery, Anhui Provincial Hospital, 17 Lujiang Road, Hefei, Anhui 230001, China

[b]Center for Hearing and Deafness, State University of New York at Buffalo, 137 Cary Hall, 3435 Main Street, Buffalo, NY 14214, USA

Abstract

High dose of salicylate, the active ingredient in aspirin, has long been known to induce transient hearing loss, tinnitus and hyperacusis making it a powerful experimental tool. These salicylate-induced perceptual disturbances are associated with a massive reduction in the neural output of the cochlea. Paradoxically, the diminished neural output of the cochlea is accompanied by a dramatic increase in sound-evoked activity in the auditory cortex (AC) and several other parts of the central nervous system. Exactly where the increase in neural activity begins and builds up along the central auditory pathway are not fully understood. To address this issue, we measured sound-evoked neural activity in the cochlea, cochlear nucleus (CN), inferior colliculus (IC), and AC before and after administering a high dose of sodium salicylate (SS, 300 mg/kg). The SS-treatment abolished low-level sound-evoked responses along the auditory pathway resulting in a 20–30 dB threshold shift. While the neural output of the cochlea was substantially reduced at high intensities, the neural responses in the CN were only slightly reduced; those in the IC were nearly normal or slightly enhanced while those in the AC considerably enhanced, indicative of a progress increase in central gain. The SS-induced increase in central response in the IC and AC was frequency-dependent with the greatest increase occurring in the mid-frequency range the putative pitch of SS-induced tinnitus. This frequency-dependent hyperactivity appeared to result from shifts in the frequency receptive fields (FRF) such that the response areas of many FRF shifted/expanded toward the mid-frequencies. Our results suggest that the SS-induced threshold shift originates in the cochlea. In contrast, enhanced central gain is not localized to one region, but progressively builds up at successively higher stage of the auditory pathway either through a loss of inhibition and/or increased excitation.

1. Introduction

Aspirin, a potent anti-inflammatory drug first synthesized by Bayer in 1897, was the mainstay treatment for rheumatoid arthritis during much of the twentieth century. Effective

*Corresponding author. Center for Hearing and Deafness, State University of New York at Buffalo, 137 Cary Hall, 3435 Main Street, Buffalo, NY 14214, USA. gchen7@buffalo.edu (G.-D. Chen).

Conflicts of interest

The authors declare no conflict of interest.

treatment of arthritic pain and inflammation required titration of the dose; a common approach involved increasing the aspirin dose until the patient experienced ringing in the ears, and then lowering it slightly until the tinnitus disappeared (Mongan et al., 1973). While aspirin is seldom used nowadays to treat arthritis, it's active ingredient, salicylate continue to be used in auditory research to investigate temporary ototoxic hearing loss and the perceptual and neural mechanisms underlying tinnitus (Bauer et al., 1999; Brennan and Jastreboff, 1991; Cazals, 2000; Chen et al., 2014a; Jastreboff and Sasaki, 1994; Jastreboff et al., 1988; Kizawa et al., 2010; Lobarinas et al., 2004; Ruttiger et al., 2003; Yang et al., 2007). Excessive sodium salicylate (SS) is thought to induce tonal tinnitus with a pitch around 10–20 kHz (Brennan and Jastreboff, 1991; Kizawa et al., 2010; Lobarinas et al., 2004; Yang et al., 2007) and recent behavioral studies indicate that salicylate also induces hyperacusis, a condition in which moderate intensity sounds are perceived as intolerably loud (Chen et al., 2014a; Zhang et al., 2014).

As with most ototoxic drugs, high-dose SS causes a cochlear hearing loss on the order of 25 dB, presumably due to its binding to prestin in the outer hair cell (OHC), which is the OHC motor protein responsible for OHC electromotility and the cochlear amplification (Kakehata and Santos-Sacchi, 1996; Rybalchenko and Santos-Sacchi, 2003). SS also greatly reduces the neural output of the cochlea as reflected in the compound action potential (CAP) which arises from the synchronized onset response of type I auditory nerve fibers (Chen et al., 2010, 2013; Stolzberg et al., 2011b; Stypulkowski, 1990; Sun et al., 2009). While the threshold shifts in the AC are comparable to the CAP suprathreshold sound-evoked responses in the AC are paradoxically much larger than normal (Chen et al., 2012, 2014a, 2013; Lu et al., 2011; Sun et al., 2009). In addition to the AC, sound-evoked hyperexcitability has also been observed in several other central structures such as the medial geniculate body and amygdala after drug or noise-induced damage to the cochlea (Chen et al., 2013, 2016; Stolzberg et al., 2011a). The hyperexcitability provides evidence for homeostatic plasticity in which the central auditory structures overcompensates for the reduced neural output of the cochlea or enhanced central gain (Auerbach et al., 2014; Norena, 2011b). Excessive central gain, resulting from diminished inhibition or increased excitation (Brummett, 1995; Gong et al., 2008; Lu et al., 2011; Sun et al., 2009; Takahashi et al., 2015; Wang et al., 2006; Xu et al., 2005), is believed to contribute to hyperacusis, loudness recruitment and subjective tinnitus (Chen et al., 2014a; Norena, 2011a). Many neurons in the AC and other auditory regions of the central nervous system also shift their frequency receptive fields (FRFs) to the mid-frequency region following SS treatment (Chen et al., 2012, 2014a; Stolzberg et al., 2011b). This imbalance and over representation of FRF may be linked to the tinnitus pitch (Chen et al., 2012). While there is clear evidence for hyperexcitability and tonotopic reorganization in central auditory structures, it is unclear whether these functional changes suddenly emerge in these regions if they are inherited in whole or in part from the lower areas of the midbrain or brainstem. To address this issues, sound-evoked responses were obtained from the cochlea, the cochlear nucleus (CN), inferior colliculus (IC) and the AC of the rat before and after administering a high dose of SS known to produce behavioral evidence of tinnitus and hyperacusis (Chen et al., 2014a; Stolzberg et al., 2012).

2. Experimental methods

2.1. Subjects

The 23 male Sprague–Dawley rats (300–500 g, Charles River Laboratories Inc.) used in this study (8 for CAP, 8 for CN, 4 for IC, and 3 for AC) were housed in the Laboratory Animal Facility (LAF) at the University at Buffalo, given free access to food and water and maintained at 22 °C on a 12-h light-dark cycle. All procedures regarding the use and handling of animals were reviewed and approved by the Institutional Animal Care and Use Committee (IACUC) at the University at Buffalo.

2.2. Sodium salicylate dosing

SS (Sigma-Aldrich, # S3007) was dissolved in sterile saline (25 mg/ml) and intraperitoneally (i.p.) injected at a dose of 300 mg/kg. Control rats received a similar volume of saline. This dose of SS has been shown to produce behavioral evidence of tinnitus and hyperacusis in rats (Chen et al., 2014a; Lobarinas et al., 2004).

2.3. Electrodes

A ring-electrode (~250 μm in diameter) made of Teflon-coated silver wire (76.2 μm in diameter, A-M systems) was placed on the round window to record cochlear compound action potential. A 16-channel linear silicon microelectrode array (A-1 × 16-10mm 100–177, NeuroNexus Technologies) was used to record sound-evoked local field potentials and multiunit clusters in CN, IC, and AC. The distance between adjacent recording electrodes on the array is 100 μm and the diameter of each electrode is 15 μm. The electrode was coated with DiI prior to insertion and the DiI label was used to confirm the location of the recording electrode from cryostat sections of CN, IC and AC as described in detail in earlier publications (Chen et al., 2013).

2.4. CAP

Tone-bursts (10 ms duration, 1 ms of rise/fall time, cosine^2-gated, 6, 8, 12, 16, 20, 24, 30 and 40 kHz) were generated by a TDT RP2.1 real-time processor (100 kHz sampling rate) and presented at 20/s. Stimuli were fed to a programmable attenuator (TDT PA5), power amplifier and high frequency transducer assembly (ACO half-inch microphone) inserted in the ear canal in front of the tympanic membrane. The transducer was calibrated in a cavity that approximated the volume of the ear canal using a microphone preamplifier (Larson Davis, model 2221) and half-inch microphone (Larson Davis, model 2540).

Rats were anesthetized with ketamine (50 mg/kg, i.p.) and xylazine (6 mg/kg, i.p.), placed on a homoeothermic blanket (Harvard Apparatus) to maintain body temperature at 37 °C and held with a custom head holder. The right bulla was surgically exposed through a ventrolateral approach, a small hole was made on the bulla to expose the round window and the electrode was placed on the round window. A silver chloride electrode was inserted into the neck muscles as a reference. The cochlear responses to tone bursts (0–90 dB SPL, 10-dB steps) were amplified (1000X) and filtered (0.1 Hz-50 kHz) using a Grass AC preamplifier (Model P15); the output of the amplifier was digitized (TDT RP2.1 real-time processor, 10.24 μs/sample), averaged 50 times and stored on a personal computer for offline analysis.

The CAP response was low-pass filtered offline (1 kHz below the tone frequency using custom MATLAB software) and the CAP amplitude was calculated as the mean value of N1-P1 and N1-P2 (see Fig. 1A).

2.5. CN, IC and AC recordings

Broadband noise bursts and tone bursts (50 ms duration, 1 ms rise/fall time, cosine^2-gating, 1–42 kHz) were generated using a TDT RX6 multifunction processor (100 kHz sampling rate) and presented with an interstimulus interval of 300 ms. The stimuli were delivered through a loudspeaker (FT28D, Fostex) located 10 cm in front of the right ear. Sound levels at the location of the animal's ear were measured with microphone preamplifier (Larson Davis, model 2221) and one-quarter inch microphone (Larson Davis, model 2520).

Rats were anesthetized with ketamine and xylazine (50 mg/kg and 6 mg/kg, i.p., respectively) and then fixed in a stereotaxic apparatus using a rat head holder and two blunted ear bars. Body temperature was maintained at 37 °C using a homoeothermic heating blanket (Harvard Apparatus). A stable plane of anesthesia was maintained with supplement doses (0.1 ml) of the ketamine-xylazine mixture (10:1 ratio) every hour. The dorsal surface of the skull was exposed and a head bar was firmly attached to the right parietal bone by a screw and dental cement. Afterwards, the right ear bar was removed permitting free-field acoustic stimulation of the right ear. An opening was made on the skull at the appropriate location to gain access to the right (ipsilateral) CN, the left (contralateral) IC, or the left (contralateral) AC. The dura was carefully opened and the 16-channel electrode array was inserted vertically into the CN, IC or AC guided by rat stereotaxic coordinates (Paxinos and Watson, 2005) and visual landmarks on the skull or surface of the brain. For CN recordings the electrode was positioned at an anterior-posterior (AP) distance of ~10.7 mm from the Bregma and a medial-lateral (ML) distance of ~4.0 mm from the midline, i.e., the posterior part of the ventral cochlear nucleus (pvCN) (see Fig. 2A). For IC recordings, the electrode was positioned at an AP distance of ~8.5 mm from Bregma and a ML distance of ~1.6 mm from the midline which targeted the central nucleus of the inferior colliculus (CIC) (see electrode penetration in Fig. 3A). For AC recording the electrode was positioned at AP 4.0 mm and ML 6.6 mm (Paxinos and Watson, 2005). The electrode array was inserted slowly from the brain surface using a FHC hydraulic microdrive until it reached an appropriate site within the CN, IC or AC as indicated by robust auditory responses on nearly all 16 recording channels.

As described previously, the biological signals were sampled with a resolution of 40.96 μs using a RA16PA preamplifier and RX5-2 pentusa base station (Tucker-Davis Technologies System-3, Alachua, FL) (Chen et al., 2014a, 2013, 2015). The signals were low-pass filtered (2–300 Hz) to obtain local field potential (LFP), which was down-sampled online with a resolution of 1.6393 ms, and simultaneously high-pass filtered (300–3500 Hz) for showing spike discharges which were detected online by using a manually set voltage threshold. The responses (LFP and discharges) to noise bursts (0–100 dB SPL, 10-dB step) were averaged 100 times. Noise burst, input/output (I/O) functions were created by off-line analysis using custom software. Responses to tone bursts were obtained at 10 frequencies (1,1.5, 2.3, 3.5, 5.3, 8,12.1,18.3, 27.7 and 42 kHz) from 0 to 100 dB SPL in 10-dB steps (50 repetitions,

pseudorandom presentation). Peri-stimulus time histograms (PSTH) were used to construct a frequency-intensity receptive field (FRF) for each multiunit cluster. After collecting 2 or 3 h of baseline recordings, SS (300 mg/kg, i.p.) was injected and then electrophysiological measurements were recorded for up to 3 h post-treatment.

2.6. SS administration

For CAP, baseline recording was obtained after the ring electrode was placed on the cochlear round window and then SS was injected (i.p.) at a dose of 300 mg/kg. After 2 h following the injection CAP was recorded again from the same electrode. For neural activity in the brain, neural responses (LFPs and discharges) to noise-bursts and tones at different frequencies and intensities were recorded after the electrode was inserted for 2 or 3 times (1 h per time) and then SS was injected (i.p.) at a dose of 300 mg/kg. The neural activity from the same electrode was continuously recorded for 4 times (post-0, 1, 2, 3 h). Post-2h means recording during 2–3 h following the SS-injection.

2.7. Electrode location

As described previously, the electrode position was verified in some animals by painting fluorescent DiI (Cat no. 42364, Sigma-Aldrich) on the surface of the electrode prior to penetration. After completing the recordings, the brain was removed, placed in 10% buffered formalin for 5–7 d, immersed in 30% sucrose solution for 2 d. Brains were cryosectioned (50 ??m) in the coronal plane. Sections were blocked in normal horse serum, incubated in a primary mouse NeuN monoclonal antibody (1:1000, Chemicon, MAB377), washed three times with phosphate buffered saline (PBS) and incubated with a donkey anti-mouse secondary antibody conjugated to Alexa Fluor 488 (1:1000; Invitrogen, A21202). Sections were washed with PBS and mounted on Superfrost slides and coverslipped with Prolong Antifade mounting medium (Invitrogen). Sections were examined and photographed using a Zeiss Axio Imager Z1 microscope equipped with a digital camera and images processed with Zeiss Axio-Vision software. The site of the recording electrode was identified by the DiI label along the electrode track in the brain slices (Examples Figs. 2A and 3A).

3. Results

3.1. CAP

Fig. 1A shows an example of CAP in response to a 12 kHz tone burst presented at 90 dB SPL before (blue solid line) and 2 h post- SS (red dashed line). The CAP N1 amplitude was greatly reduced 2 h post-SS. CAP I/O functions were measured before and after the treatment with 300 mg/kg SS (n = 5) or an equal volume of saline (n = 3). There was a very slight reduction in CAP amplitude 2 h post-saline which not statistically significant (data not shown) whereas CAP amplitudes were greatly reduced after SS treatment at all frequencies. To provide a global perspective on the SS-induced changes, a mean CAP I/O function was computed for all test frequencies from 6 to 40 kHz before and 2 h post-SS. Prior to SS treatment, the mean (±-SEM, n = 5, Fig. 1B) CAP amplitude increased monotonically with intensity reaching a mean maximum amplitude of around 110 μV at 90 dB SPL (blue open circles). The mean CAP I/O function measured 2 h post-SS (red filled circles) was shifted to the right of the pre-SS function. The rightward shift at a 5 μV potential (the smallest

recognizable CAP) was roughly 25 dB indicative of mild threshold shift (Fig. 1B, horizontal dashed arrow). More importantly, mean CAP amplitudes were greatly reduced at suprathreshold intensities. At 90 dB SPL, the mean amplitude decreased from approximately 110 μV–30 μV, a decrease of nearly 70% (Fig. 1B, vertical dashed arrow). A two way ANOVA (40–90 dB SPL) showed a significant effect of SS-treatment ($F = 1403$, 1, 234 DF; $p < 0.0001$) and also SS-treatment × intensity interaction ($F = 144.7$, 5, 234 DF, $p < 0.0001$). A Bonferroni post-hoc analysis indicated that the post-SS amplitudes were significantly less than pre-exposure values from 50 to 90 dB SPL ($p < 0.001$). To determine if the amplitude reduction was frequency dependent, the mean (±SEM) percent reduction in CAP amplitude between 60 and 90 dB SPL was computed for each frequency at 2 h post-SS and the values plotted as a function of frequency (Fig. 1C). SS caused large decreases in CAP amplitude, 50–70%, across a broad range of frequencies. The decreases in the low-frequency range (≤16 kHz) were ~50–55%, but were more severe (~60–70%) in the high-frequency range.

3.2. CN LFP

The sound-evoked LFP was recorded from an electrode located in the posterior ventral cochlear nucleus (pvCN). Fig. 2A is an example showing DiI mark of a recording electrode passing through dorsal cochlear nucleus (dCN) into the pvCN. Representative CN-LFP waveforms evoked with noise-bursts presented at intensities from 40 to 100 dB SPL are shown in Fig. 2B pre (black solid line) and 2 h post-SS (red dashed line). After SS treatment, the CN LFP at 40 dB SPL was absent. At 60 and 80 dB SPL, the post-SS LFP amplitudes were greatly reduced and response latency delayed while at 100 dB SPL, the post-SS and pre-SS amplitude and latency were nearly the same. To quantify the SS-induced change in amplitude, the root mean square (RMS) of the LFP was determined over a 50 ms response window. Fig. 2C presents the mean (±-SEM) RMS amplitude of the CN LFP as a function of intensity. Mean data are shown from 43 recording sites in 6 rats pre- (black open circles) and 2 h post-SS (red filled circles) and from 18 recording sites in 2 rats pre- and 2 h post-saline. The CN LFP input/output functions remained unchanged after saline injection (data not shown). However, the CN LFP input/output functions were dramatically altered 2 h post-SS. At low-intensities, the post-SS input/output function was shifted to the right approximately 25 dB (at 5 μV), similar to the threshold shift seen for the CAP. As intensity increased, the amplitude of the post-SS CN LFP increased at a slightly faster rate than normal rate, particularly between 80 and 100 dB SPL. Consequently, the response amplitude at 100 dB was only slightly less than pre-SS. This is remarkable given that the CAP amplitude was reduced by nearly 70%. A two way ANOVA (40–100 dB SPL) showed a significant effect of SS-treatment ($F = 357.1$, 1, 294 DF; $p < 0.0001$) and also a significant SS-treatment × intensity interaction ($F = 5.76$, 6, 294 DF, $p < 0.0001$). A Bonferroni post-hoc analysis indicated that the post-SS amplitudes were significantly less than pre-exposure values from 40 to 90 dB SPL, but not at 100 dB SPL.

To identify possible frequency dependent changes, the CN LFP amplitudes were measured across frequency and intensity pre- and 2 h post-SS. The percent change in CN LFP amplitude was computed relative to pre-treatment baseline and plotted as a function of frequency. The average (±SEM) percent reduction in CN LFP amplitude is shown in Fig. 2D for intensities from 60 to 100 dB SPL. The mean (±-SEM) SS-induced reductions in the CN

were approximately 20% across the entire frequency range. The reductions in the CN were independent of frequency and the reductions were substantially less than for the CAP.

3.3. IC LFP

Sound-evoked LFPs were measured from electrodes in the central nucleus of the IC (CIC) as indicated by the DiI labeling of the electrode penetration (Fig. 3A). Fig. 3B shows representative IC LFP waveforms obtained from the CIC in response to noise bursts presented at different levels pre- (black solid lines) and 2 h post-SS (red dashed lines). The IC LFP at 40 dB SPL was greatly reduced 2 h post-SS consistent with the peripheral hearing loss. However the IC LFP amplitudes at 60, 80 and 100 dB SPL were larger than control values in contrast to the CAP or CN-LFP. Fig. 3C shows the mean (±-SEM) RMS amplitude (50 ms window) of 40 IC LFP recordings in 4 rats in response to noise bursts presented at intensities from 0 to 100 dB SPL. At low intensities (<40 dB SPL) IC LFP responses were greatly reduced 2 h post-SS (red filled circles) resulting in a threshold shift of ~25 dB (horizontal arrow). However, at intensities from 60 to 100 dB SPL, the responses were significantly enhanced 10–15%. A two way ANOVA (60–100 dB SPL) showed a significant enhancive effect of SS-treatment ($F = 114, 1, 195$ DF; $p < 0.0001$), but no significance of SS-treatment × intensity interaction ($F = 0.88, 4, 195$ DF, $p = 0.48$).

To determine if the amplitude enhancements were frequency dependent, the mean (±SEM, n = 40 recording sites in 4 rats) IC LFP amplitudes elicited by tone bursts were measured across frequency and intensity pre and 2 h post-SS. The percent changes in IC LFP amplitude (±-SEM) relative to pre-treatment baseline were computed and plotted as a function of frequency (Fig. 3D). At 100 dB SPL (black open squares), LFP amplitudes were enhanced 5–20% up to 12.1 kHz, followed by a 5–15% decrease at higher frequencies. At 60 and 80 dB SPL (red filled squares), a somewhat similar enhancement pattern was observed. In contrast to the CN-reduction of 20%, the IC LFP at 60 and 80 dB SPL showed a 15–20% enhancement at the mid-frequencies.

3.4. AC LFP

Fig. 4A presents representative AC LFP waveforms in response to noise bursts at 40, 60, 80 and 100 dB SPL pre- (black solid lines) and 2 h post-SS (red dashed lines). LFP amplitudes were greater at 60, 80, and 100 dB SPL 2 h post-SS compared to the pre-SS response, but reduced at 40 dB SPL. Fig. 4B presents mean LFP RMS (50 ms window) of 42 recordings in the AC of 3 rats in response to noise bursts of increasing intensity. The responses at low-stimulus levels were reduced and the threshold shifted to the right ~20 dB (horizontal arrow). However, LFP amplitudes increased rapidly above 40 dB SPL resulting in significantly enhanced responses at the high stimulation levels. A two way ANOVA (50–100 dB SPL) showed a significant enhancive effect of SS-treatment ($F = 1098, 1, 246$ DF; $p < 0.0001$) and also a significant SS-treatment × intensity interaction ($F = 38.01, 5, 246$ DF, $p < 0.0001$) indicating a sound-level-dependent SS-effects. A Bonferroni post-hoc analysis indicated that the post-SS amplitudes were significantly greater than pre-exposure values from 50 to 100 dB SPL ($p < 0.001$). AC LFPs were measured with tone bursts (50 ms) to determine if the amplitude enhancement varied with frequency. Fig. 4C presents the mean (±SEM, 42 recordings, 3 rats) percent change in AC LFP amplitude for intensities from 60

to 100 dB SPL. In contrast to more peripheral loci, the SS-enhancement of AC LFP amplitude occurred at all frequencies with the greatest enhancement occurring approximately between 12 and 28 kHz.

3.5. Multiunit cluster in CN and IC

The changes in LFP amplitude were strongly frequency dependent in the AC. To investigate potential peripheral sources for this effect, we measured the spike discharge patterns from multiunit clusters in response to tone bursts (50 ms) presented over a range of frequencies (1–42 kHz) and intensities (0–100 dB, 10 dB steps). We used the data to construct a matrix of PSTH (200 ms window) that mapped out the frequency receptive field (FRF) of multiunit clusters in the CN and IC and used this to construct tuning curves and discharge rate-intensity functions.

Fig. 5A and B shows the frequency-intensity matrix of PSTHs for a multiunit cluster recorded in the CN pre- and 2 h post-SS. The baseline characteristic frequency (CF) of this multiunit cluster was ~1.5 kHz and the CF-threshold was approximately 20 dB SPL (Fig. 5A). The CF of this multiunit cluster was essentially unchanged 2 h post-SS even though the CF-threshold had increased 20–30 dB (Fig. 5B). Fig. 5C presents the discharge rate (50 ms window) versus intensity functions for tone bursts presented at CF (1.5 kHz) and 12.1 kHz (mid-frequency) pre- and 2 h post-SS. The discharge rate-intensity functions were shifted to the right approximately 20 dB, a threshold shift similar to that for the CAP. Results similar to this were obtained from other multiunit clusters tuned to other CFs indicating that the threshold shift was inherited from the periphery. The discharge rates at 1.5 and 12.1 kHz were reduced at all suprathreshold intensities. Suprathreshold reductions in firing rate similar to this were observed from other multiunit clusters consistent with the hypoactivity observed in CN LFPs (Fig. 2D).

Fig. 6A and B presents the frequency-intensity matrix of PSTH for a multiunit cluster in the IC pre- and 2 h post-SS. This multiunit cluster had a CF near 1.5 kHz and a CF-threshold of 20 dB SPL (6A). PSTH responses extending over the duration of the stimulus were mainly confined to frequencies of 1 and 1.5 kHz. The features of the PSTH matrix changed dramatically 2 h post-SS. Thresholds at frequencies near the pre-treatment CF of 1.5 kHz increased ~20 dB (up-arrow, Fig. 6B). Surprisingly, the PSTH matrix expanded toward the high frequencies and high frequency thresholds decreased by as much as 30–40 dB (down-arrow Fig. 6B). The frequency-dependent increase and decrease in threshold altered the spectral profile of the PSTH matrix leading to a shift in CF from 1.5 kHz to 5.3 kHz. In addition, the high-frequency PSTH were much broader post-SS. For example, at 5.3 kHz, the pre-treatment PSTH mainly consisted of an onset response (6A) whereas the post-SS PSTH was broader and extended over the duration of the stimulus (6B). Fig. 6C shows the discharge rate-intensity function of this multiunit cluster at CF (1.5 kHz, 50 ms tone bursts). The pre-treatment firing rate (black open circles) increased with intensity above 10 dB SPL and reached a quasi-saturation rate between 50 and 100 dB SPL. The discharge rate-intensity function 2 h post-SS (red filled circles) was shifted to the right approximately 20 dB (horizontal line) consistent with the peripheral threshold shift (Fig. 1). The firing rates at low-stimulus levels (<50 dB SPL) were lower than normal, but at high intensities the

responses were substantially above pre-treatment values (up-arrow). The discharge rate-intensity function at 5.3 kHz from the same multiunit cluster is shown in Fig. 6D. The pre-treatment input/output function increased monotonically above 40 dB SPL (black open circles). At 2 h post-SS, discharge rates were enhanced over a broad range of intensities (Fig. 6D, solid up-arrow) even to intensities below the pre-treatment threshold (Fig. 6D, up dashed arrow). This resulted in a threshold decrease of approximately 20 dB SPL (Fig. 6D, horizontal arrow). PSTH matrix of this multiunit cluster was measured 3 times before SS-treatment (pre-1, 2, and 3 h) and 3 times post-SS treatment (post-1, 2, and 3 h). Tuning curves of the multiunit cluster were obtained from the PSTH matrixes and the pre-SS tuning curves (Fig. 6E, black open circles) and the post-SS tuning curves (Fig. 6E, red filled circles) were averaged (±SEM). At frequencies near the original CF (1.5 kHz), thresholds increased approximately 20 dB (up arrowhead) whereas at frequencies several octave above the original CF, thresholds decreased substantially (down arrowhead). This resulted in a rightward shift of the FRF post-SS. Fig. 6F shows the mean FRF of seven low-CF multiunit clusters pre- (black open circles) and 2 h post-SS. The pre-SS thresholds were lowest (~20 dB SPL) in the 1–2.3 kHz range and increased substantially at higher frequencies. At 2 h post-SS, the low-frequency thresholds increased approximately 20 dB (up arrowhead) whereas high-frequency thresholds decreased substantially (down arrowhead). A two-way ANOVA revealed significant pre-post threshold differences ($F = 13.52$, 1, 60 DF, $p = 0.0005$) and a significant SS-treatment × frequency interaction ($F = 13.03$, 9, 60 DF, $p < 0.0001$). A Bonferroni post-hoc analysis revealed significant post-SS threshold increases in the pre-CF range ($p < 0.05$) and significant post-SS thresholds decreases in the high-frequency range.

Unlike low-CF neurons, SS failed to induce an up shift in the CF of mid-CF multiunit clusters as illustrated in Fig. 7A. This multiunit cluster had a CF near 12.1 kHz and a CF-threshold of ~20 dB (black open circles) before SS treatment. Post-SS treatment (red filled circles), the thresholds near CF had increased 10–20 dB; thresholds in the low-frequency tail were elevated less resulting in a slight downward shift in CF. Fig. 7B presents the discharge rate-intensity function (50 ms tone bursts) at the original CF of 12.1 kHz. At low intensities, the rate-level function was shifted to the right 20–30 dB and discharge rates were below normal. However, discharge rates at suprathreshold levels (>50 dB SPL) were consistently greater than baseline control. These trends were evident in the mean FRF of seven IC multiunit clusters with CF at 12.1 or 18.3 kHz (Fig. 7C). The mean CF of the FRFs was 12.1 kHz and the CF-threshold was 20 dB SPL. At 2 h post-SS, the mean response thresholds had increased significantly except at 5.3 kHz. A two-way ANOVA revealed significant pre-post threshold differences ($F = 303.8$, 1, 60 DF, $p < 0.0001$) and a significant SS-treatment × frequency interaction ($F = 9.04$, 9, 60 DF, $p < 0.0001$). A Bonferroni post-hoc analysis revealed significant post-SS threshold increases at all the frequencies except 5.3 kHz. Because the threshold shifts were greater near the tip of the original FRF, there was slight down shift in CF to 8 kHz and broadening of the low-threshold tip of the mean FRF.

Fig. 8A shows a representative FRF of a high-CF IC multiunit cluster which had a CF of 27.7 kHz and a CF-threshold of 20 dB before treatment (open circle). At 2 h post-SS, thresholds had increased considerably near the tip of the FRF (27.7 kHz), but were largely unaffected from 5.3 to 12.1 kHz resulting in a broad tip to the FRF. The discharge rate-intensity function (50 ms window) at the original CF (27.7 kHz) was shifted to the right

approximately 20 dB after SS treatment (Fig. 8B, horizontal arrow) and the discharge rates were reduced at all intensities (down arrow) unlike the mid- and low-CF neurons (Figs. 6–7). However, the discharge rate-intensity function at 12.1 kHz, where there was little threshold shift, was largely unaffected post-SS (Fig. 8C). Fig. 8D shows the mean FRF from 12 high-CF multiunit clusters in the IC; the mean CF was near 27.7 kHz and the CF-threshold was slightly less than 20 dB (black open circles). Thresholds at high-frequencies near CF (18.3–42 kHz) were elevated significantly whereas the low-frequency thresholds were largely unaffected. A two-way ANOVA revealed significant pre-post threshold differences ($F = 151.2, 1, 110$ DF, $p < 0.0001$) and a significant SS-treatment × frequency interaction ($F = 14.77, 9, 110$ DF, $p < 0.0001$). A Bonferroni post-hoc analysis revealed significant post-SS threshold increases at 18.3, 27.7 and 42 kHz ($p < 0.001$). The two dominant changes seen in high CF multiunit clusters, namely more threshold shift near CF than below CF and a greater reduction in firing rate above CF than below CF, leads to a relative enhancement of mid-frequency activity at the expense of the high-frequencies.

3.6. Multiunit cluster in AC

Frequency receptive fields and discharge rate-intensity functions were also recorded from multiunit clusters in the AC, but the results will not be reported here since they have been discussed in detail in earlier reports (Chen et al., 2013; Stolzberg et al., 2011b; Sun et al., 2009). Briefly, SS elevated AC thresholds at the CF of multiunit clusters by 20–30 dB; the magnitude of the threshold shifts were similar to those seen at the level of the cochlea, CN and IC, results indicative of a cochlear hearing loss. Firing rates at CF were reduced at low intensities, but greatly enhanced at supra-threshold intensities. These results were similar to those seen in the IC except that the magnitude of the enhancement tended to be larger in the AC than the IC. SS produced large frequency dependent changes in AC FRF. The CF of many low-CF multiunit clusters in the AC tended to shift up towards the mid frequencies (10–20 kHz); this was accompanied by upward shift in the high-frequency side of the FRF and an increase in threshold at frequencies at and/or below the original CF. The changes were similar to, but tended to be more pronounced than, those seen in the IC (Fig. 6). The CF of many high-CF multiunit clusters in the AC tended to shift downward towards the mid frequencies (10–20 kHz); this was caused by a decrease in threshold at frequencies below the high-frequency edge of the original FRF. These changes were similar, but more pronounced than those seen in high-CF multiunit clusters in the IC (Fig. 8).

4. Discussion

The neural hyperactivity and frequency map reorganization that occurs in the central auditory center after treatment with high dose SS have been documented previously (Chen and Jastreboff, 1995; Chen et al., 2012, 2013, 2014a, 2014b; Deng et al., 2010; Lu et al., 2011; Norena et al., 2010; Stolzberg et al., 2011b; Sun et al., 2009; Zhang et al., 2011). However, the neural origins of these phenomena and the extent to which more peripheral structures such as the CN and IC contribute to these changes are poorly understood. The current study identified several relevant findings. (1) Although sound-evoked neural activity in the CN was reduced post-SS, the magnitude of this reduction was proportionately less than in the cochlear CAP (Fig. 9) suggesting that compensatory neural amplification is

occurring in CN to compensate for the reduced output from the cochlea. (2) Neural amplification in the CN, however, was largely independent of frequency. (3) Suprathreshold sound-evoked hyperactivity was first seen in the IC. (4) IC sound-evoked hyperactivity was frequency dependent with the largest enhancement (~25%) occurring around 10–20 kHz. (5) Suprathreshold sound-evoked hyperactivity occurred at all frequencies in the AC, but the greatest enhancement (~85%) occurred between 10 and 20 kHz. (5) CF upshifts in low-frequency multiunit clusters and slight CF downshifts in high frequency multiunit clusters was first observed in the IC, but never seen in the CN. (6) The CF upshifts and downshifts in FRF were more pronounced in the AC than the IC. Collectively, the results suggest that the compensatory gain increase begins in the CN and progressively increase along the ascending auditory pathway, i.e., cumulative increase in central gain originating at multiple levels of auditory processing. On the other hand, the CF upshifts and downshifts in FRF begin in the IC and became more pronounced in the AC. Together, these two factors combine to enhance suprathreshold activity in the AC particularly in the 10–20 kHz region (Fig. 9).

4.1. SS-induced threshold shift and cochlear hypoactivity

Our 300 mg/kg dose of SS induced a CAP threshold shift of 20–30 dB (Fig. 1). The magnitude of the threshold shift is consistent with earlier reports in several different species (Cazals, 2000; Chen et al., 2013; Guitton et al., 2003; Muller et al., 2003) and is presumably due to the effect of SS on OHCs. SS is believed to induce temporary hearing loss by binding to prestin expressed in the OHC, reducing electromotility, cochlear amplification and distortion product otoacoustic emissions (Chen et al., 2010, 2013; Kakehata and Santos-Sacchi, 1996; Rybalchenko and Santos-Sacchi, 2003; Stolzberg et al., 2011b; Yamanishi et al., 2008). The magnitude of threshold shift in the LFPs recorded in the CN, IC and AC were similar to the CAP suggesting that the loss of auditory threshold observed in the cochlea is propagated centrally.

SS also significantly reduced CAP amplitudes at suprathreshold levels in a frequency dependent manner. The largest decreases were observed at high frequencies and less at frequencies below 20 kHz (Fig. 1C) consistent with previous reports (Chen et al., 2013; Muller et al., 2003). The cochlear basal turn is known to be more vulnerable to many ototoxic drugs than the apical turn. The mechanisms that lead to this diminished output from the auditory nerve are poorly understood. At the cellular level, SS potentiates NMDA-mediated synaptic transmission through glutamatergic receptors in SGN allowing the influx of calcium (Peng et al., 2003). In cochlear cultures, high doses of SS destroyed auditory nerve fibers and induced TUNEL staining and caspase-mediated cell death in SGN but paradoxically failed to damage hair cells (Deng et al., 2013; Wei et al., 2010; Zheng and Gao, 1996). Magnesium partially blocked SGN degeneration suggesting that cell death was partially medicated by calcium-influx through NMDA receptors. In vivo, SS altered the rate and temporal pattern of spontaneous activity in auditory nerve fibers and reduced the neural input to the central auditory pathway (Cazals et al., 1998; Muller et al., 2003; Ruel et al., 2008).

4.2. CN compensation

If the auditory pathway were a simple transmission line, the hypoactivity leaving the cochlea would be expected to reduce the level of activity in the CN to a similar degree. Fig. 9 compares the percentage decreases or increases in suprathreshold LFP amplitudes across frequency in the auditory nerve (CAP), CN, IC and AC. Suprathreshold CAP amplitudes were reduced by approximately 70% at high frequencies and 50% at low frequencies (black filled inverse triangles, Fig. 9), a reduction of similar magnitude and spectral profile might expected in the CN. Contrary to expectation, sound evoked responses in the CN (blue open inverse triangles, Fig. 9) were only reduced 20% across the entire frequency range, substantially less than the CAP. Suprathreshold discharge rates from CN multiunit clusters were also a reduced to a moderate degree across a broad range of CFs consistent with LFP amplitude measures (Fig. 5). The results suggest that a compensatory boost is occurring in the CN. The amplification could arise from synaptic changes or loss of inhibition. After acute acoustic trauma above CF, increase in firing rate was observed in a subset of neurons in the dorsal CN (DCN) with narrow excitatory response areas surrounded by inhibitory sidebands (Salvi et al., 2000a), evidence consistent with a loss of lateral inhibition. Chronic *in vivo* treatment with SS increased the number of synaptic vesicles, the length of postsynaptic densities as well as GAP-43 and GFAP immunolabeling in the VCN (Fang et al., 2016). These changes were interpreted as evidence of increased excitatory synapses in the VCN designed to compensate for the reduced neural response from the cochlea. Homeostatic plasticity has been observed in bushy cells in the anteroventral cochlear nucleus following chronic, non-damaging sound stimulation (Ngodup et al., 2015). In measurements of excitatory postsynaptic currents in brain slices, prolonged noise stimulation decreased the probability of release and an increased in number of release sites. This was accompanied anatomically by an increase in the size of afferent endbulb and the number of postsynaptic densities per profile. These results demonstrate that the level of sound evoked activity can dramatically alter the excitability at synapses that relays activity between the auditory nerve and the CN. Pre and post-synaptic homeostatic mechanisms similar to this have also been found to modulate synaptic efficiency and gain in several other forms of cochlear hearing loss (Mendoza Schulz et al., 2014; Oleskevich and Walmsley, 2002; Taberner and Liberman, 2005).

4.3. Frequency-dependent hyperactivity in IC and AC

SS significantly enhanced suprathreshold sound-evoked LFPs in the IC in a frequency dependent manner. Despite the large reductions in the CAP and moderated decreases in the CN, supra-threshold IC responses were normal at the low frequencies, 25% larger than normal in the 10–20 kHz range, but slightly reduced at high frequencies (Fig. 3). The frequency dependent enhancement of suprathreshold activity was even greater and extended over a broader frequency range in the AC. Suprathreshold responses were now enhanced at all frequency (Fig. 9). Suprathreshold LFP amplitudes were 50% larger than normal at low frequencies, nearly 100% larger at the mid frequencies and 25% greater at high frequencies. A graphical model that accounts for several aspects of the data is shown in Fig. 10. The magnitude of neural activity in each low, mid and high CF multiunit clusters is portrayed by the height of each block and the number of blocks; the color of each block indicates the original CF. The normalized LFP amplitude pre-SS has a value of 1 in each frequency band

(equal number of blocks, same size) (Fig. 10A). Values > 1 are indicated by (+) and values < 1 are indicated by (−). Post-SS suprathreshold firing rates were typically higher than normal in all three frequency bands in both the IC and AC (increase in height of each block) (Fig. 10B). This boost in firing rate likely accounts for the large global increase in LFP amplitude seen in the AC. The large response enhancements in the AC reflects the summation of gain inherited from lower levels of the auditory pathway plus those in the AC.

The SS-induced LFP enhancement was frequency dependent with the largest increase occurring in the mid frequency range. SS often induced a large CF upshift among low CF multiunit clusters, a moderate CF downshift in high CF multiunit clusters and little change in mid-CF clusters. These CF upshifts and downshift were only observed in the AC and IC, but not the CN. This is schematized in Fig. 10B by CF upshifts (blue blocks) and downshifts (red bocks) of multiunit clusters that also have enhanced discharge rates. These CF upshifts and downshifts presumably contribute to frequency specific enhancement of LFP amplitudes at the mid frequencies. The frequency dependent enhancement of suprathreshold activity was greater and more widespread in the AC than the IC. The large mid-frequency enhancements in the AC reflects the summation of gain inherited from lower levels plus the frequency dependent CF shifts inherited from the IC and those in the AC.

The mechanisms that lead to the CF upshifts and downshifts in the AC and IC are poorly understood. Despite the fact that most neurons in the central auditory pathway exhibit sharp tuning, there is growing evidence that some of these neurons integrate information over a larger frequency range than reflected in their excitatory FRF. Many neurons in the auditory cortex show a dramatic expansion of their FRF, decreases in threshold and increases in suprathreshold firing rate when GABA-mediated inhibition is suppressed (Wang et al., 2002a, 2002b). The FRF of neurons in the central auditory pathway often undergo dramatic changes following cochlear damage. For example, sharply tuned neurons in the AC, IC and DCN show an expansion of their excitatory response areas following acoustic trauma (Scholl and Wehr, 2008); these changes can occur even when a traumatizing tone is presented far above CF suggesting that high frequencies far above CF suppress sound evoked response at and below CF (Salvi et al., 2000b; Wang et al., 1996). The frequency expansion and hyperactivity is thought to result from the loss of inhibition, consistent with the reduction of GABA-mediated inhibition seen after acoustic trauma (Milbrandt et al., 2000). Local SS application is known to reduce GABAergic inhibition in the brain (Bauer et al., 2000; Gong et al., 2008; Wang et al., 2006; Xu et al., 2005). Moreover, infusion of SS into the amygdala significantly enhances sound evoked activity in the AC without inducing a threshold shift, strong evidence for a central mediated effect (Chen et al., 2012, 2014a).

4.4. Hyperacusis

In addition to inducing tinnitus with a putative pitch near 10–20 kHz (Brennan and Jastreboff, 1991; Kizawa et al., 2010; Lobarinas et al., 2004; Yang et al., 2007), our recent results show that high doses of SS also induce hyperacusis, a condition in which moderate intensity sounds are perceived as intolerably loud or painful (Chen et al., 2014a, 2015; Hayes et al., 2014). Our results from the AC indicate that SS-induced hyperactivity occurs over a broad frequency range (Fig. 4). These results are consistent with our behavioral

measures of hyperacusis obtained using broadband noise bursts. However, the SS-induced hyperactivity in the AC has a distinct spectral profile. Suprathreshold responses show far greater enhancement in the 10–20 kHz range than at lower frequencies. These results lead to the hypothesis that behavioral measures of hyperacusis measured with frequency specific tone bursts will be more severe when measured with 16 kHz tones than hyperacusis measured with higher and lower frequencies, a prediction consistent with our preliminary behavioral results.

4.5. Synopsis

SS induced a cochlear hearing loss of approximately 20 dB, but also reduced the sound-evoked neural output of the cochlea by more than 50%. The threshold shift observed at the cochlea was recapitulated at higher levels of the auditory pathway. In contrast, the suprathreshold sound-evoked responses in the AC were much larger at all frequencies, but having a spectral peak at the mid frequencies with maximum enhancement of nearly 100%. The hyperactivity observed in the AC is derived from two factors. The first is a frequency-independent neural amplification which begins in the CN and build ups at successively higher levels of the auditory pathway. While the mechanisms underlying this frequency-independent amplification are poorly understood, activity-dependent, synaptic plasticity that increases excitatory neuro-transmission is a plausible candidate (Ngodup et al., 2015). The second factor, a frequency-dependent amplification, most likely results from pronounced CF upshifts of low-CF multiunit clusters and moderate downshifts of high-CF multiunit clusters. CF upshifts and downshifts emerged in the IC and became more pronounced in the AC. Such changes are likely mediated by diminished inhibition that allows the full range of spectral inputs to be expressed when the suppressive effects of lateral inhibition are removed (Salvi et al., 2007; Scholl et al., 2008; Wang et al., 2002a; Wang et al., 2002b; Wehr and Zador, 2003).

Acknowledgments

Research supported in part by grants from NIH (R01DC014452 and R01DC014693).

Abbreviations

AC	auditory cortex
AP	anterior-posterior
CAP	compound action potential
CF	characteristic frequency
CIC	central nucleus of inferior colliculus
CN	cochlear nucleus
FRF	frequency receptive field
IC	inferior colliculus

I/O	input/output
LFP	local field potential
ML	medial-lateral
N1	first negative peak of CAP
OHC	outer hair cell
PSTH	peristimulus time histogram
pvCN	posterior ventral cochlear nucleus
RMS	root mean square
SS	sodium salicylate

References

Auerbach BD, Rodrigues PV, Salvi RJ. Central gain control in tinnitus and hyperacusis. Front Neurol. 2014; 5:206. [PubMed: 25386157]

Bauer CA, Brozoski TJ, Holder TM, Caspary DM. Effects of chronic salicylate on GABAergic activity in rat inferior colliculus. Hear Res. 2000; 147:175–182. [PubMed: 10962183]

Bauer CA, Brozoski TJ, Rojas R, Boley J, Wyder M. Behavioral model of chronic tinnitus in rats. Otolaryngol Head Neck Surg. 1999; 121:457–462. [PubMed: 10504604]

Brennan JF, Jastreboff PJ. Generalization of conditioned suppression during salicylate-induced phantom auditory perception in rats. Acta Neurobiol Exp. 1991; 51:15–27.

Brummett, RE. A mechanism for tinnitus?. In: Vernon, J., Moller, A., editors. Mechanisms of Tinnitus. Allyn and Bacon; MA: 1995. p. 7-10.

Cazals Y. Auditory sensori-neural alterations induced by salicylate. Prog Neurobiol. 2000; 62:583–631. [PubMed: 10880852]

Cazals Y, Horner KC, Huang ZW. Alterations in average spectrum of cochleoneural activity by long-term salicylate treatment in the Guinea pig: a plausible index of tinnitus. J Neurophysiol. 1998; 80:2113–2120. [PubMed: 9772265]

Chen GD, Jastreboff PJ. Salicylate-induced abnormal activity in the inferior colliculus of rats. Hear Res. 1995; 82:158–178. [PubMed: 7775282]

Chen GD, Manohar S, Salvi R. Amygdala hyperactivity and tonotopic shift after salicylate exposure. Brain Res. 2012; 1485:63–76. [PubMed: 22464181]

Chen GD, Sheppard A, Salvi R. Noise trauma induced plastic changes in brain regions outside the classical auditory pathway. Neuroscience. 2016; 315:228–245. [PubMed: 26701290]

Chen GD, Radziwon KE, Kashanian N, Manohar S, Salvi R. Salicylate-induced auditory perceptual disorders and plastic changes in nonclassical auditory centers in rats. Neural Plast. 2014a; 2014:658741. [PubMed: 24891959]

Chen GD, Stolzberg D, Lobarinas E, Sun W, Ding D, Salvi R. Salicylate-induced cochlear impairments, cortical hyperactivity and re-tuning, and tinnitus. Hear Res. 2013; 295:100–113. [PubMed: 23201030]

Chen GD, Kermany MH, D'Elia A, Ralli M, Tanaka C, Bielefeld EC, Ding D, Henderson D, Salvi R. Too much of a good thing: long-term treatment with salicylate strengthens outer hair cell function but impairs auditory neural activity. Hear Res. 2010; 265:63–69. [PubMed: 20214971]

Chen YC, Zhang J, Li XW, Xia W, Feng X, Gao B, Ju SH, Wang J, Salvi R, Teng GJ. Aberrant spontaneous brain activity in chronic tinnitus patients revealed by resting-state functional MRI. Neuroimage Clin. 2014b; 6:222–228. [PubMed: 25379434]

Chen YC, Li X, Liu L, Wang J, Lu CQ, Yang M, Jiao Y, Zang FC, Radziwon K, Chen GD, Sun W, Krishnan Muthaiah VP, Salvi R, Teng GJ. Tinnitus and hyperacusis involve hyperactivity and enhanced connectivity in auditory-limbic-arousal-cerebellar network. Elife. 2015; 4:e06576. [PubMed: 25962854]

Deng A, Lu J, Sun W. Temporal processing in inferior colliculus and auditory cortex affected by high doses of salicylate. Brain Res. 2010; 1344:96–103. [PubMed: 20451503]

Deng L, Ding D, Su J, Manohar S, Salvi R. Salicylate selectively kills cochlear spiral ganglion neurons by paradoxically up-regulating superoxide. Neurotox Res. 2013; 24:307–319. [PubMed: 23494753]

Fang L, Fu Y, Zhang TY. Salicylate-induced hearing loss trigger structural synaptic modifications in the ventral cochlear nucleus of rats via medial olivocochlear (MOC) feedback Circuit. Neurochem Res. 2016; 41:1343–1353. [PubMed: 26886762]

Gong N, Zhang M, Zhang XB, Chen L, Sun GC, Xu TL. The aspirin metabolite salicylate enhances neuronal excitation in rat hippocampal CA1 area through reducing GABAergic inhibition. Neuropharmacology. 2008; 54:454–463. [PubMed: 18078964]

Guitton MJ, Caston J, Ruel J, Johnson RM, Pujol R, Puel JL. Salicylate induces tinnitus through activation of cochlear NMDA receptors. J Neurosci. 2003; 23:3944–3952. [PubMed: 12736364]

Hayes SH, Radziwon KE, Stolzberg DJ, Salvi RJ. Behavioral models of tinnitus and hyperacusis in animals. Front Neurol. 2014; 5:179. [PubMed: 25278931]

Jastreboff PJ, Sasaki CT. An animal model of tinnitus: a decade of development. Am J Otol. 1994; 15:19–27. [PubMed: 8109625]

Jastreboff PJ, Brennan JF, Coleman JK, Sasaki CT. Phantom auditory sensation in rats: an animal model for tinnitus. Behav Neurosci. 1988; 102:811–822. [PubMed: 3214530]

Kakehata S, Santos-Sacchi J. Effects of salicylate and lanthanides on outer hair cell motility and associated gating charge. J Neurosci. 1996; 16:4881–4889. [PubMed: 8756420]

Kizawa K, Kitahara T, Horii A, Maekawa C, Kuramasu T, Kawashima T, Nishiike S, Doi K, Inohara H. Behavioral assessment and identification of a molecular marker in a salicylate-induced tinnitus in rats. Neuroscience. 2010; 165:1323–1332. [PubMed: 19958810]

Lobarinas E, Sun W, Cushing R, Salvi R. A novel behavioral paradigm for assessing tinnitus using schedule-induced polydipsia avoidance conditioning (SIP-AC). Hear Res. 2004; 190:109–114. [PubMed: 15051133]

Lu J, Lobarinas E, Deng A, Goodey R, Stolzberg D, Salvi RJ, Sun W. GABAergic neural activity involved in salicylate-induced auditory cortex gain enhancement. Neuroscience. 2011; 189:187–198. [PubMed: 21664433]

Mendoza Schulz A, Jing Z, Sanchez Caro JM, Wetzel F, Dresbach T, Strenzke N, Wichmann C, Moser T. Bassoon-disruption slows vesicle replenishment and induces homeostatic plasticity at a CNS synapse. EMBO J. 2014; 33:512–527. [PubMed: 24442636]

Milbrandt JC, Holder TM, Wilson MC, Salvi RJ, Caspary DM. GAD levels and muscimol binding in rat inferior colliculus following acoustic trauma. Hear Res. 2000; 147:251–260. [PubMed: 10962189]

Mongan E, Kelly P, Nies K, Porter WW, Paulus HE. Tinnitus as an indication of therapeutic serum salicylate levels. JAMA. 1973; 226:142–145. [PubMed: 4740906]

Muller M, Klinke R, Arnold W, Oestreicher E. Auditory nerve fibre responses to salicylate revisited. Hear Res. 2003; 183:37–43. [PubMed: 13679136]

Ngodup T, Goetz JA, McGuire BC, Sun W, Lauer AM, Xu-Friedman MA. Activity-dependent, homeostatic regulation of neurotransmitter release from auditory nerve fibers. Proc Natl Acad Sci U S A. 2015; 112:6479–6484. [PubMed: 25944933]

Norena AJ. An integrative model of tinnitus based on a central gain controlling neural sensitivity. Neurosci Biobehav Rev. 2011a; 35:1089–1109. [PubMed: 21094182]

Norena AJ. An integrative model of tinnitus based on a central gain controlling neural sensitivity. Neurosci Biobehav Rev. 2011b; 35:1089–1109. [PubMed: 21094182]

Norena AJ, Moffat G, Blanc JL, Pezard L, Cazals Y. Neural changes in the auditory cortex of awake Guinea pigs after two tinnitus inducers: salicylate and acoustic trauma. Neuroscience. 2010; 166:1194–1209. [PubMed: 20096752]

Oleskevich S, Walmsley B. Synaptic transmission in the auditory brainstem of normal and congenitally deaf mice. J Physiol. 2002; 540:447–455. [PubMed: 11956335]

Paxinos, G., Watson, C. The Rat Brain in Stereotaxic Coordinates. 5. 2005.

Peng BG, Chen S, Lin X. Aspirin selectively augmented N-methyl-D-aspartate types of glutamate responses in cultured spiral ganglion neurons of mice. Neurosci Lett. 2003; 343:21–24. [PubMed: 12749988]

Ruel J, Chabbert C, Nouvian R, Bendris R, Eybalin M, Leger CL, Bourien J, Mersel M, Puel JL. Salicylate enables cochlear arachidonic-acid-sensitive NMDA receptor responses. J Neurosci. 2008; 28:7313–7323. [PubMed: 18632935]

Ruttiger L, Ciuffani J, Zenner HP, Knipper M. A behavioral paradigm to judge acute sodium salicylate-induced sound experience in rats: a new approach for an animal model on tinnitus. Hear Res. 2003; 180:39–50. [PubMed: 12782351]

Rybalchenko V, Santos-Sacchi J. Cl- flux through a non-selective, stretch-sensitive conductance influences the outer hair cell motor of the Guinea-pig. J Physiol. 2003; 547:873–891. [PubMed: 12562920]

Salvi RJ, Wang J, Ding D. Auditory plasticity and hyperactivity following cochlear damage. Hear Res. 2000a; 147:261–274. [PubMed: 10962190]

Salvi RJ, Wang J, Ding D. Auditory plasticity and hyperactivity following cochlear damage. Hear Res. 2000b; 147:261–274. [PubMed: 10962190]

Salvi, RJ., Wang, J., Caspary, D. Functional changes in the central auditory system after noise-induced cochlear damage. In: Luxon, L., Prasher, D., editors. Noise and its Effects. John Wiley & Sons; London, England: 2007. p. 110-126.

Scholl B, Wehr M. Disruption of balanced cortical excitation and inhibition by acoustic trauma. J Neurophysiol. 2008; 100:646–656. [PubMed: 18525018]

Scholl B, Gao X, Wehr M. Level dependence of contextual modulation in auditory cortex. J Neurophysiol. 2008; 99:1616–1627. [PubMed: 18216226]

Stolzberg D, Chen GD, Allman BL, Salvi RJ. Salicylate-induced peripheral auditory changes and tonotopic reorganization of auditory cortex. Neuroscience. 2011a; 180:157–164. [PubMed: 21310217]

Stolzberg D, Chen GD, Allman BL, Salvi RJ. Salicylate-induced peripheral auditory changes and tonotopic reorganization of auditory cortex. Neuroscience. 2011b; 180:157–164. [PubMed: 21310217]

Stolzberg D, Chrostowski M, Salvi RJ, Allman BL. Intracortical circuits amplify sound-evoked activity in primary auditory cortex following systemic injection of salicylate in the rat. J Neurophysiol. 2012; 108:200–214. [PubMed: 22496535]

Stypulkowski PH. Mechanisms of salicylate ototoxicity. Hear Res. 1990; 46:113–145. [PubMed: 2380120]

Sun W, Lu J, Stolzberg D, Gray L, Deng A, Lobarinas E, Salvi RJ. Salicylate increases the gain of the central auditory system. Neuroscience. 2009; 159:325–334. [PubMed: 19154777]

Taberner AM, Liberman MC. Response properties of single auditory nerve fibers in the mouse. J Neurophysiol. 2005; 93:557–569. [PubMed: 15456804]

Takahashi S, Ukai S, Tsuji T, Ueyama T, Kono M, Yamanaka N, Shinosaki K. Reduction of cortical excitability and increase of thalamic activity in a low-frequency rTMS treatment for chronic tinnitus. Neurocase. 2015; 21:339–344. [PubMed: 24606019]

Wang HT, Luo B, Zhou KQ, Xu TL, Chen L. Sodium salicylate reduces inhibitory postsynaptic currents in neurons of rat auditory cortex. Hear Res. 2006; 215:77–83. [PubMed: 16632286]

Wang J, Salvi RJ, Powers N. Plasticity of response properties of inferior colliculus neurons following acute cochlear damage. J Neurophysiol. 1996; 75:171–183. [PubMed: 8822550]

Wang J, McFadden SL, Caspary D, Salvi R. Gamma-aminobutyric acid circuits shape response properties of auditory cortex neurons. Brain Res. 2002a; 944:219–231. [PubMed: 12106684]

Wang J, McFadden SL, Caspary D, Salvi R. Gamma-aminobutyric acid circuits shape response properties of auditory cortex neurons. Brain Res. 2002b; 944:219–231. [PubMed: 12106684]

Wehr M, Zador AM. Balanced inhibition underlies tuning and sharpens spike timing in auditory cortex. nature. 2003; 426:442–446. [PubMed: 14647382]

Wei L, Ding D, Salvi R. Salicylate-induced degeneration of cochlea spiral ganglion neurons-apoptosis signaling. Neuroscience. 2010; 168:288–299. [PubMed: 20298761]

Xu H, Gong N, Chen L, Xu TL. Sodium salicylate reduces gamma aminobutyric acid-induced current in rat spinal dorsal horn neurons. Neuroreport. 2005; 16:813–816. [PubMed: 15891576]

Yamanishi Y, Kitaura J, Izawa K, Matsuoka T, Oki T, Lu Y, Shibata F, Yamazaki S, Kumagai H, Nakajima H, Maeda-Yamamoto M, Tybulewicz VL, Takai T, Kitamura T. Analysis of mouse LMIR5/CLM-7 as an activating receptor: differential regulation of LMIR5/CLM-7 in mouse versus human cells. Blood. 2008; 111:688–698. [PubMed: 17928527]

Yang G, Lobarinas E, Zhang L, Turner J, Stolzberg D, Salvi R, Sun W. Salicylate induced tinnitus: behavioral measures and neural activity in auditory cortex of awake rats. Hear Res. 2007; 226:244–253. [PubMed: 16904853]

Zhang C, Flowers E, Li JX, Wang Q, Sun W. Loudness perception affected by high doses of salicylate–a behavioral model of hyperacusis. Behav Brain Res. 2014; 271:16–22. [PubMed: 24882611]

Zhang X, Yang P, Cao Y, Qin L, Sato Y. Salicylate induced neural changes in the primary auditory cortex of awake cats. Neuroscience. 2011; 172:232–245. [PubMed: 21044658]

Zheng JL, Gao WQ. Differential damage to auditory neurons and hair cells by ototoxins and neuroprotection by specific neurotrophins in rat cochlear organotypic cultures. Eur J Neurosci. 1996; 8:1897–1905. [PubMed: 8921280]

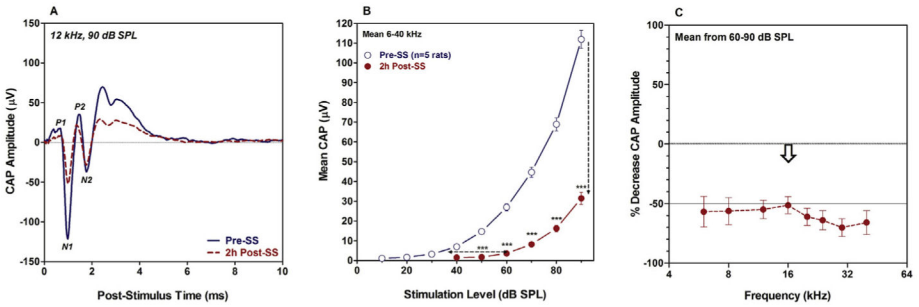

Fig. 1.

SS suppressed the amplitude of the compound action potential (CAP). (A) CAP waveform elicited by 12 kHz tone burst presented at 90 dB SPL pre-SS (blue solid line) and 2 h post-SS (red dashed line). CAP amplitude is the mean of N_1-P_1 and N_1-P_2. (B) Mean (± SEM, n = 5) amplitude of CAP pre-SS (blue open circles) and 2 h post-SS (red filled circles). Data averaged across frequencies of 6–40 kHz. Asterisks indicate pre-post differences that were statistically significant. (C) Mean (± SEM, n = 5 rats) percentage decrease in CAP amplitude at intensities from 60 to 90 dB SPL measured 2 h post-SS plotted as a function of frequency.

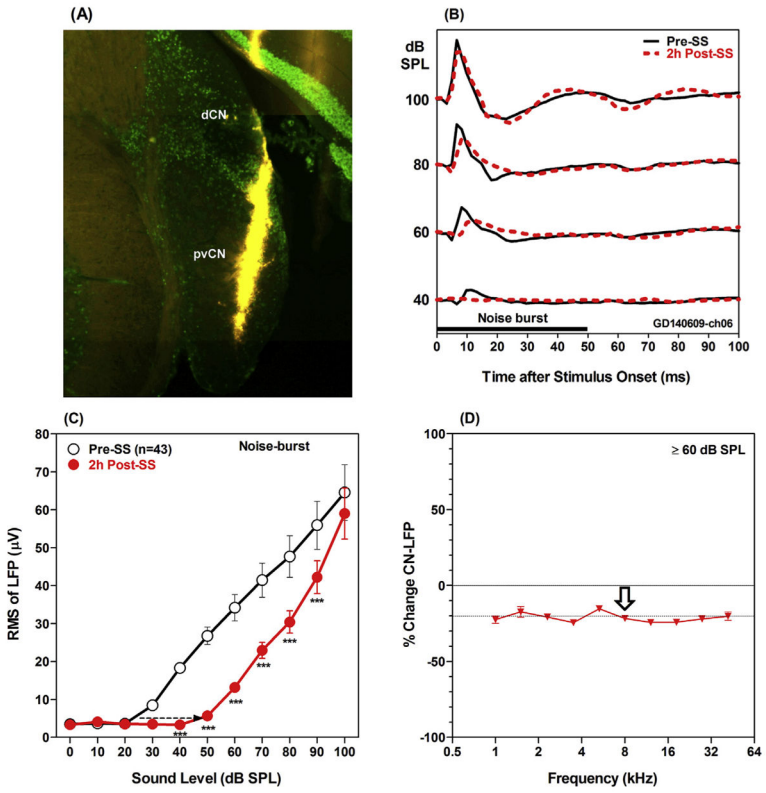

Fig. 2.

SS induced changes in CN LFP amplitude. (A) Photomicrograph showing fluorescent DiI (red) mark of the location of the multichannel electrode in the posterior-ventral cochlear nucleus (pvCN). Fluorescent (green) NeuN antibody used to label neurons. (B) Representative LFP waveforms in the pvCN elicited by noise bursts (50 ms duration, 1 ms rise/fall time) at intensities from 40 to 100 dB SPL. Data show pre- (black solid lines) and 2 h post-SS treatment (red dashed lines). (C) Mean (± SEM, n = 43) CN LFP amplitude as a function of intensity pre- (black open circles) and 2 h post-SS (red filled circles). Asterisks indicate pre-post differences that were statistically significant. (D) Average (± SEM, n = 43) percent change in CN LFP amplitude for intensities from 60 to 100 dB SPL plotted as a function of frequency.

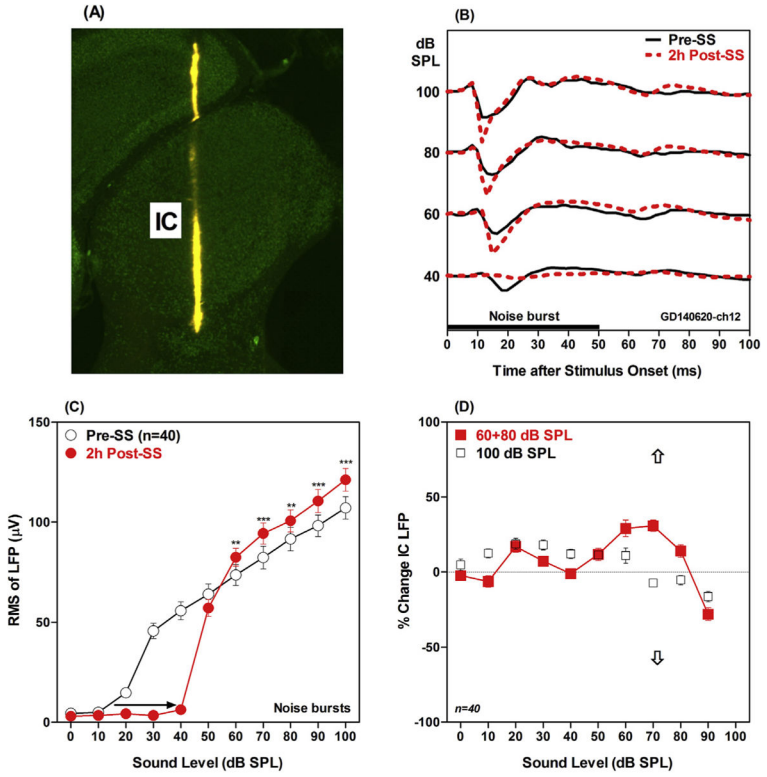

Fig. 3.

SS Induced change in IC LFP amplitude. (A) Photomicrograph showing fluorescent DiI (red) mark of the location of the multichannel electrode in the central nucleus of the inferior colliculus. Fluorescent (green) NeuN antibody used to label neurons. (B) Representative LFP waveforms in the central nucleus of the IC elicited by noise bursts (50 ms duration, 1 ms rise/fall time) at intensities from 40 to 100 dB SPL. Data shown pre- (black solid lines) and 2 h post-SS (red dashed lines). (C) Mean (± SEM, n = 40) RMS IC LFP amplitude as a function of intensity pre- (black open circles) and 2 h post-SS (red filled circles). Asterisks indicate pre-post increases that were significant greater than pre-treatment. (D) Average (± SEM, n = 43) percent change in IC LFP RMS amplitude for intensities of 60 plus 80 dB SPL and 100 dB SPL plotted as a function of frequency.

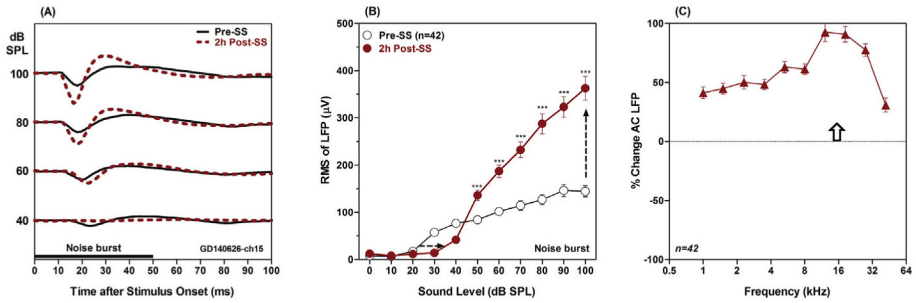

Fig. 4.

SS Induced change in AC LFP amplitude. (A) Representative LFP waveforms in the primary AC elicited by noise bursts (50 ms duration, 1 ms rise/fall time) at intensities from 40 to 100 dB SPL. Data shown pre- (black solid lines) and 2 h post-SS (red dashed lines). (B) Mean (± SEM, n = 42) IC LFP amplitude as a function of intensity pre- (black open circles) and 2 h post-SS (red filled circles). Asterisks indicate pre-post increases that were significantly greater than pre-treatment. (C) Average (± SEM, n = 42) percent change in AC LFP amplitude for intensities from 60 to 100 dB SPL plotted as a function of frequency.

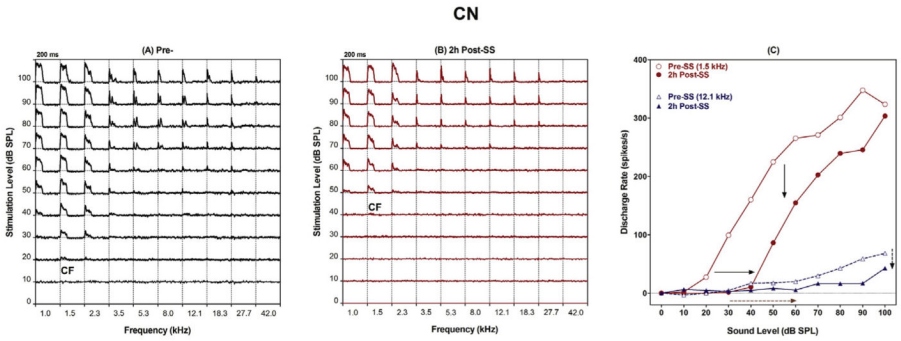

Fig. 5.

SS suppressed sound-evoked responses in the cochlear nucleus (CN). Frequency-intensity matrix of PSTH for a typical multiunit cluster in the CN (A) pre- and (B) 2 h post-SS. (A) Pre-characteristic frequency (CF) ~1.5 kHz; CF-threshold ~20 dB. (B) Post-CF unchanged even though the CF-threshold increased 20–30 dB; (C) Mean discharge rate (50 ms window)-intensity functions at CF (1.5 kHz) and 12.1 kHz pre- and 2 h post-SS. Firing rate decreased at all suprathreshold intensities (down arrows) and rate-intensity functions shifted to the right approximately 20 dB (horizontal arrow).

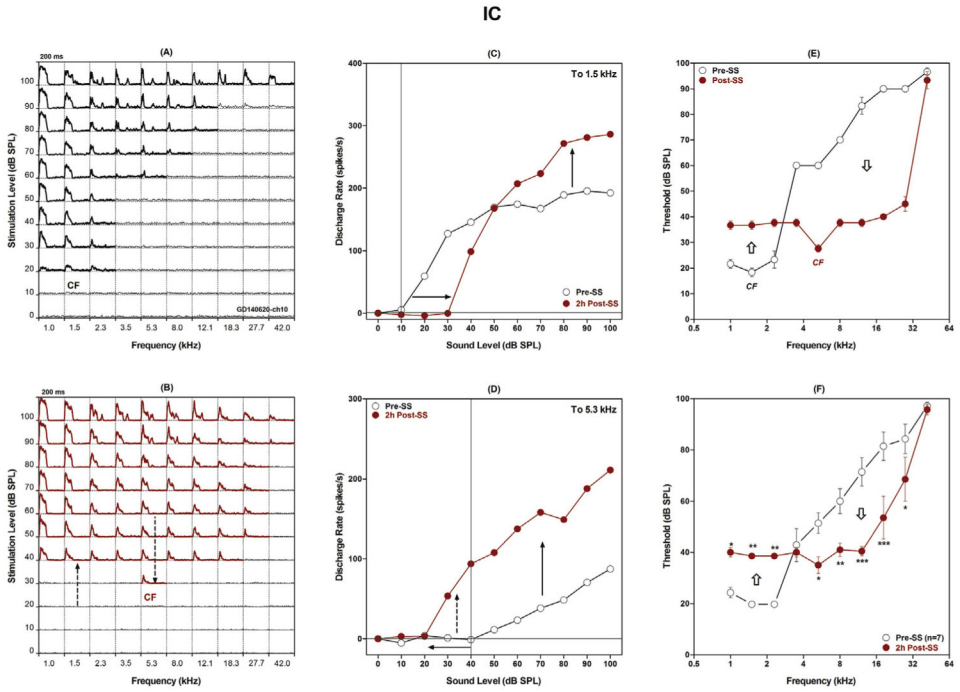

Fig. 6.

SS induced CF shift and enhanced firing rates in low-frequency IC multiunit clusters. (A) Baseline (Pre) frequency-intensity matrix of PSTH of a multiunit cluster. Each cell shows the PSTH (200 ms window) elicited with 50 ms tone bursts at the designated frequency-intensity combination. Pre-treatment CF was ~1.5 kHz and CF-threshold was approximately ~20 dB SPL. (B) Frequency-intensity matrix of PSTH of the multiunit cluster obtained 2 h post-SS. Note threshold increases of approximately 20 dB from 1 to 2.3 kHz (up arrow) and threshold decreases of 20 dB or more from 3.5 to 18.3 kHz (down arrow). (C) Discharge rate-intensity function of the IC multiunit cluster at 1.5 kHz pre- (black open circles) and 2 h post-SS (red filled circles). Note a response threshold at 10 dB SPL (vertical line) and ~20 dB threshold loss 2 h post-SS (rightward arrow) and increase in suprathreshold firing rates (up arrow). (D) Discharge rate-intensity function of the IC multiunit cluster at 5.3 kHz pre- (black open circles) and 2 h post-SS (red filled circles). Note a response threshold at 40 dB SPL (vertical line) and ~20 dB gain of response threshold 2 h post-SS (leftward arrow) and increase in firing rate at suprathreshold intensities (solid up arrow) and sound levels previously below threshold (dashed up arrow). (E) Mean of 3 pre-SS FRFs (collected during 3 h prior to the SS-treatment from this representative multiunit cluster, black open circles) and of 3 post-SS FRFs (post-1h, 2 h, and 3 h, red filled circles). Note threshold increases (up arrow) of approximately 20 dB near 1.5 kHz and large threshold decreases (down arrow) at higher frequencies that resulted an upward shift in CF post-SS from ~1.5 kHz to 5.3 kHz. (F) Mean (± SEM) FRFs of seven low-CF multiunit cluster measured pre- (black open circles) and 2 h post-SS (red filled circles). Note SS-induced threshold increases (up arrow) of approximately 20 dB from 1 to 2.3 kHz and large threshold decreases (down arrow) at higher frequencies. Asterisks indicate pre-post changes that were significantly different from pre-treatment.

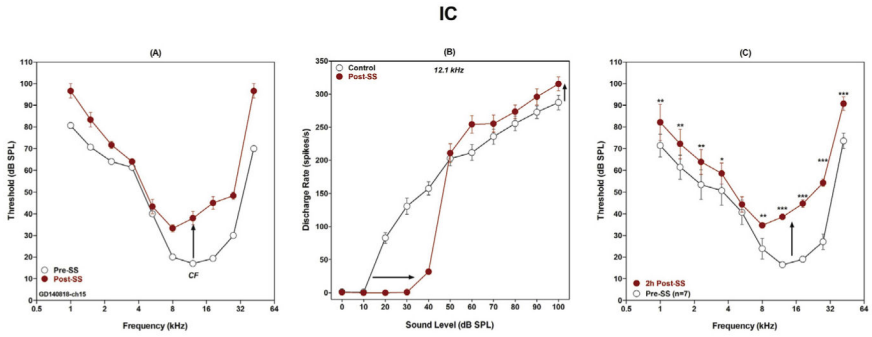

Fig. 7.

SS induced threshold shift in mid-frequency IC multiunit clusters but enhanced discharge rates at high stimulation levels. (A) Mean of 3 pre-SS FRFs (collected during 3 h prior to the SS-treatment from a representative multiunit cluster, black open circles) and 3 post-SS FRFs (post-1h, 2 h, and 3 h, red filled circles) of the cluster. CF near 12.1 kHz and CF-threshold ~20 dB. Note threshold increase (up arrow) of approximately 20 dB around the CF that resulted in a slight downshift in CF. (B) Discharge rate-intensity function of the IC multiunit cluster at 12.1 kHz pre- (black open circles) and 2 h post-SS (red filled circles). Note ~20 dB thresholds shift 2 h post-SS (horizontal line) and increase in suprathreshold firing rates (up arrow). (C) Mean (± SEM) frequency receptive fields of seven mid-CF multiunit clusters measured pre- (black open circles) and 2 h post-SS (red filled circles). Note significant SS-induced threshold increases (up arrow) of approximately 20–30 dB at 12.1 kHz and higher, 10–15 dB threshold shifts below 4 kHz and minimal change at 5.3 kHz.

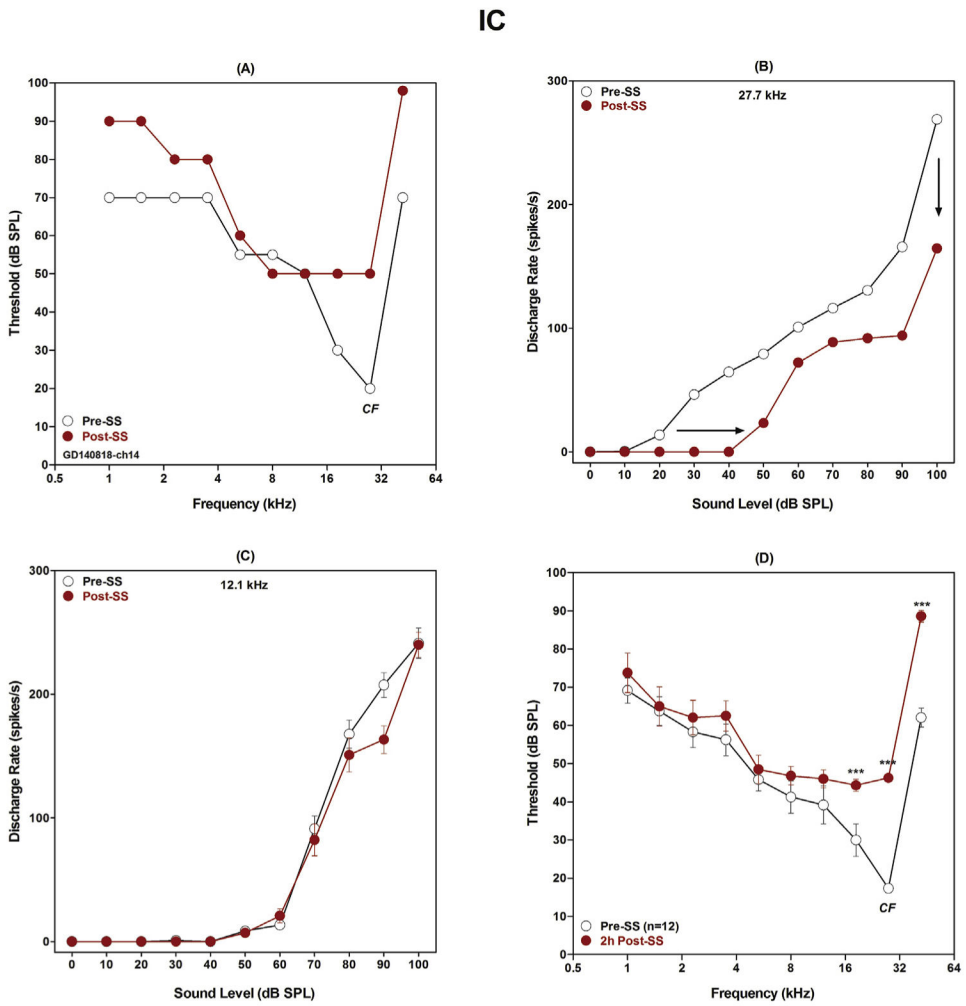

Fig. 8.

SS induced threshold shift in high-frequency IC multiunit clusters. (A) Frequency receptive field from a representative high-CF IC multiunit cluster pre- and 2 h post-SS. Pre-CF near 27.7 kHz and CF-threshold ~20 dB. Note threshold increase of 20–30 dB around the CF, 10–20 dB at low frequencies, and less than 5 dB at the frequencies of 5.3–12.1 kHz that resulted in a broad tip and slight downshift in tuning. (B) Discharge rate-intensity function of the IC multiunit cluster at 27.7 kHz pre- (black open circles) and 2 h post-SS (red filled circles). Note ~20 dB thresholds shift 2 h post-SS (horizontal arrow) and decrease in suprathreshold firing rates at all levels (down arrow). (C) Discharge rate intensity function at 12.1 kHz of the multiunit cluster; note largely unchanged response amplitude post-SS. (D) Mean (± SEM) frequency receptive fields of 12 high-CF multiunit clusters in IC measured pre- (black open circles) and 2 h post-SS (red filled circles). Note significant SS-induced threshold increases of 10–30 dB around and above the original CF, but insignificant increase at low frequencies.

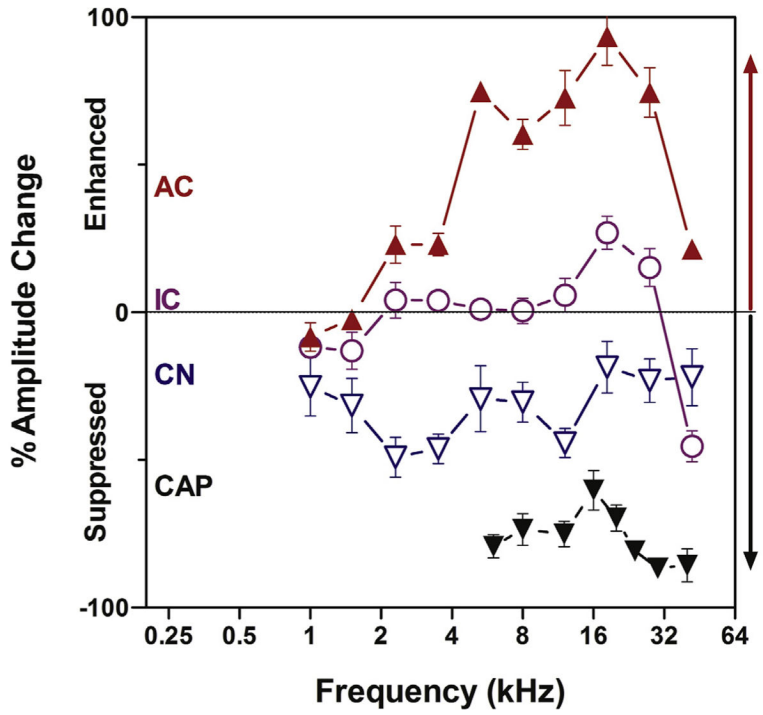

Fig. 9.

SS-induced changes of tone-evoked CAP and local field potentials along the auditory pathway. All measurements obtained at 80 dB SPL. Data shown more reduction in the cochlea (CAP, black filled inverse triangles), less reduction in the cochlear nucleus (CN, blue open inverse triangles), divergent changes in the inferior colliculus (CN, purple open circles) with an increase in the mid-frequency range, and increase in the auditory cortex (AC, red filled triangles) with the greatest increase in the mid-frequency region.

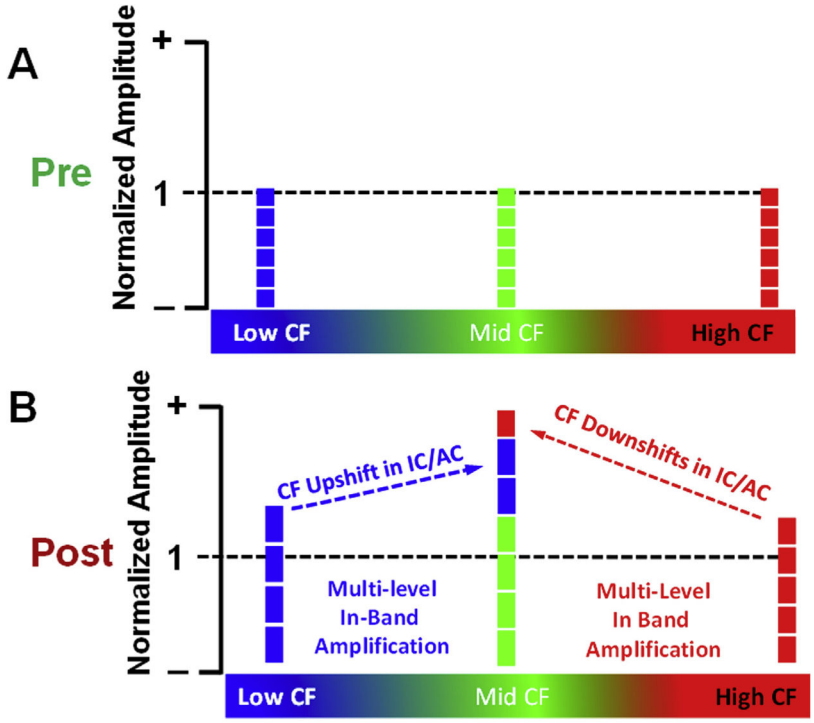

Fig. 10.

Graphical model of SS-induced frequency-dependent hyperactivity. (A) Normalized amplitudes of neural activity in auditory cortex produced by suprathreshold neurons with low, mid and high CFs pre-treatment. (B) SS induces multi-level in-band amplification of sound evoked activity in low, mid and high CF neurons at multiple level from the cochlear nucleus to auditory cortex resulting in hyperactivity across all frequency bands in auditory cortex. The CF upshifts of low CF neurons and CF downshift of high CF neurons preferentially enhances sound-evoked activity in the mid-frequency region.